Construction and Characterization of a Pump Source for a Microchip Laser for Space Applications

Bruno Couto, Paulo Gordo and António Amorim
CENTRA-SIM, Faculty of Sciences of the University of Lisbon, Campo Grande 1749-016 Lisbon, Portugal

Keywords: Pulsed Laser, Laser Pumping Optics, Small Lens Systems.

Abstract: In the context of an apparent increasing interest in remote exploration of rocky celestial bodies, a pulsed microchip laser for time-of-flight range finding applications is under development. This paper addresses the design construction and testing of the pump source for this laser unit. Considering the small mass, miniature size and high pump power the space application requires, open emitter semiconductor lasers become the only real option as a main pumping source. However, this type of geometry is limited by a beam profile with significantly different divergence values on the fast and slow axes. We endeavoured to correct this issue by collimating each of the axis independently. After a design and simulation stage, the lenses were mounted in front of the main pump source with the aid of a custom made wavefront sensor.

1 INTRODUCTION

There is a growing interest in the study and exploration of rocky bodies, either planets or asteroids, accessible to spacecrafts (ESRE, 2017). The mission costs involved in getting a scientific payload to a celestial body drive the development of all support instrumentation toward miniaturization as is the case of landing control systems (Hitoshi and Kawaguchi 2011). In this context, our group is developing a small sized pulsed laser source that can be used in a miniaturized laser time-of-flight range finder.

During this project stage, an engineering model is to be achieved that emits pulses with up to 100µj and a pulse width of some ns. The whole laser unit is also to be subjected to limited environmental testing which mainly materialize in thermal vacuum cycling between -40°C and 50°C at a pressure of 10^{-6} mbar. Vibration or static load are not in the scope of the current development and may be addressed at a new project.

The laser source in development is a Microchip Laser. The initial Microchip laser concept, proposed by Zayhowski et al., consisted of very narrow diode pumped solid state laser cavity with the cavity mirrors directly coated onto the active medium faces (Zayhowski and Mooradian, 1989). Q-switched Microchip laser systems were soon to appear (Zayhowski et al., 1989) and these can be implemented with a saturable absorbers (Hamlin et al., 2004), as is the case of our design.

The required 1.5µm emission wavelength range drove our design selection toward an Yb-Er:glass active medium with a Co:Spinel saturable absorber. The pump band of Yb-Er:glass has a peak around 975nm, matching a very common emission wavelength for semiconductor lasers.

Considering the goal of a miniaturized laser system, fiber coupled diode-lasers were not considered a design option due to the footprint necessities of accomodating a spool of fiber. Laser diodes housed in a TO type package are commercially available and may emcompass convient support devices such as photodiodes or temperature sensors. However lasers in this type of housing emitt a beam that differently diverges on the vertical and horizontal axes. The correction of this feature is typically hampered by the casing window which limits the proximity at which beam conditioning optics may be placed.

Open emitter laser diodes present a convenient solution in what concerns size and, although they also output a beam with the same diferential divergence predicament as the TO packaged lasers, the placement of correction optics is unemcumbered. Of the available open emmiter options C-Mounted laser diodes stand out by not requiring chip soldering and

Couto, B., Gordo, P. and Amorim, A.
Construction and Characterization of a Pump Source for a Microchip Laser for Space Applications.
DOI: 10.5220/0007400602130219
In *Proceedings of the 7th International Conference on Photonics, Optics and Laser Technology (PHOTOPTICS 2019)*, pages 213-219
ISBN: 978-989-758-364-3

allowing simple assembly and were therefore the choice for this developemnt.

The current literature addresses several approaches for focusing or collimating the output of open emmiter laser diodes such as using graded index lenses (Johansson et al., 2007), holographic lenses (Bouguin and Galstian, 2002) and several different types of custom optics (Hasan et al., 2016). However, we could not find many references for the practical implementation of a system based on common off-the-shelf optics. By presenting this paper we aim at covering that gap, thereby facilitating this type of development for other engineers and scientists.

The very short length of the active medium of this design (~1.5mm) demands considerable concentration of the pump beam in order to reach gain values that may enable high energy pulses.

This paper details the approach taken to re-shape the beam, the optical design, the method used to optimize the positioning of the lenses and the comparison of the design with the obtained results.

2 OPTICAL DESIGN OF THE PUMP SYSTEM

The pump source selected for this design was a II-VI Laser Enterprise SEC9-9xx75-01. This laser diode outputs an astigmatic beam with an elliptic profile that diverges by approximately 40º on the fast axis and by 14º on slow axis. The emitter width is specified to be of 90µm while its height is estimated to be of the typical value of 1µm (Sun, 2015).

Passively Q-switched Microchip Laser implementations published for the same materials and with comparable output values (Mlynczak and Belghachem, 2015) use a circular the pump beam spot diameter between 100µm and 200µm. Owing to the comparatively low thermal conductivity of the glass active medium used (0.7W/m.K), the circularity of the pump beam becomes relevant as differential heat deposition profile between the fast and slow axis of pump beam may translate into a correspondently asymmetric thermal lensing. Hence the drive for this design was to circularize the beam as much as possible and focus it to a diameter within the above-mentioned range.

2.1 Beam Shaping Approach

To correct the asymmetric propagation profile, the straightforward approach of collimating each of the axis independently with perpendicularly placed cylindrical lenses was taken. In doing so, care was taken that each of the axis was collimated at the same diameter as depicted in the schematic on Figure 1

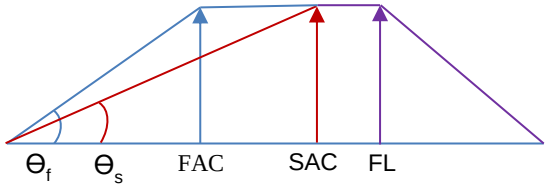

Figure 1: Schematic for the beam shaping approach.

In Figure 1 Θ_f stands for the fast axis divergence, Θ_s stands for the slow axis divergence, *FAC* stands for the fast axis collimator and *SAC* stands for the slow axis collimator and FL for the focusing lens. Both axes are represented in the same plane for simplicity.

2.2 Optical System Design

Considering a chosen fast axis collimator, and the edge ray height at the lens principal plane h_1 was simply calculated as

$$h_1 = f_{FAC}\, tan(\theta_f) \tag{1}$$

where f_{FAC} represents the fast axis collimator focal length. Subsequently, the focal length of a matching slow axis collimator was calculated as

$$f_{SAC} = \frac{h_1}{tan(\theta_s)} \tag{2}$$

So, the set of target specifications for the optics presented in Table 1 could be considered.

Table 1: Target Specifications for the Optical System.

Θ_f (˚)	Θ_s (˚)	f_{FAC} (mm)	h_1 (mm)	f_{SAC} (mm)
19.55	6.8	2.2	0.781	6.165

2.2.1 Sequential Ray-tracing Simulations

A selection of commercially available lenses that more closely matched the target specifications in Table 1 was considered for sequential ray-tracing simulations in Zemax. This optic selection was composed of three different models of cylindrical lenses for the fast axis collimator, another three for the slow axis collimator and two different models of spherical lenses for the focal lens.

All possible combinations of FAC, SAC and FL within this set were simulated. The vertical and lateral dimensions of the emitter were simulated by using

three different fields for each direction. The position of the FAC of each combination was optimized through a merit function to provide the most collimated beam possible in that direction and after the same was made for the SAC. The FL was simply placed at 1mm distance from the SAC. As the fast and slow axis did not focus in the same spot, the distance from the focusing lens that minimized both axes was sought through a merit function as well. The position obtained was the considered as the focal length of the system. The dimensions of the pump spot were assessed through footprint diagrams like the one presented in Figure 2, which outlines the cross section of the selected fields at a given surface.

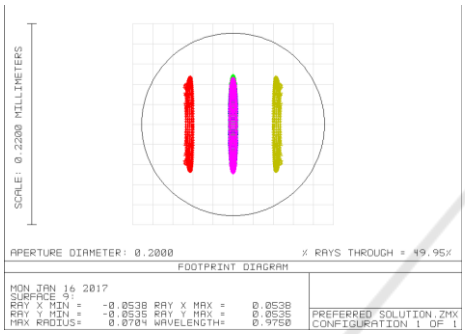

Figure 2: Footprint Diagram at the focal spot of the system.

The optical design presented in Figure 3 was the best trade-off between short length and the most circular beam at the focal area i.e. the smallest difference between beam width and height.

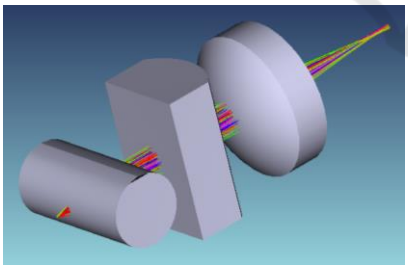

Figure 3: Shaded Model of the Optical Design.

The main characteristics of the optical system selected are presented in Table 2.

Table 2: Main Characteristics of the Optical System Designed.

f_{FAC} (mm)	f_{SAC} (mm)	f_{FL} (mm)	*Pump Spot dimensions (μm)*	*System length (mm)*
2.2	5.8	6	108x108	16.2

Both the SAC and the FL are AR coated for the significant wavelength range. The materials of the selected lenses are respectively BK7, N-BK7 and N-SF11.

The total ionising dose estimated for the Curiosity Rover electronic parts was of 6.8kRad (Kemski, 2011). This can reasonably be assumed to be a conservative reference for our system since it is meant to be integrated in landing support instrumentation. Such a dose has been shown to degrade the transmissivity of these glasses or very similar ones in less than 5% at 975nm wavelength (Manolis et al., 2015); (Akhtar et al., 2007), meaning that radiation compatibility will not be a major risk for the optics.

2.2.2 Non-sequential Ray-tracing Simulations

Although a major contribution from backscattering effects is not expected, the practical approach of a non-sequential simulation was taken as it provides data relevant for further stages of the laser model development.

A laser source with characteristics matching those mentioned above was defined and the selected lens models were placed at the positions optimized in sequential mode.

An intensity profile of the beam was taken at the system focal length defined with sequential optimization. It is depicted in Figure 4.

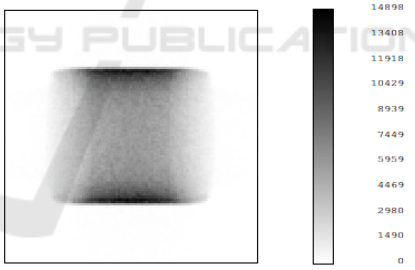

Figure 4: Beam profile at focal length.

Two horizontal lobes on the upper and lower limits of the beam profile can be distinguished. Further simulations allowed to detect that this effect first appears at the FAC output. The beam spans 104μm vertically and 127μm horizontally, which is not a complete match for the sequential result but is still within the required dimensions. Similar simulations were carried out with variations of 0.1mm from the focal region to verify the behaviour of the beam along its propagation axis, the results for which are plotted in Figure 5. These also indicate that the smallest difference in beam width for the two axes occurs near 4.75mm from FL.

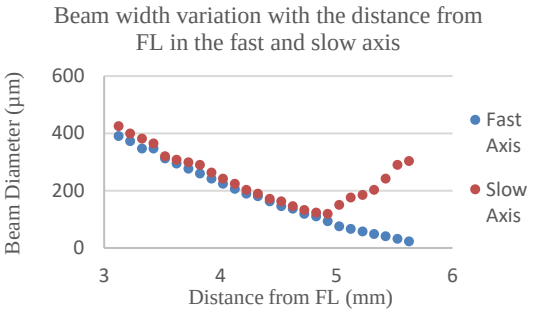

Figure 5: Non-Sequential results for beam width variation along propagation direction.

3 ASSEMBLY OF THE OPTICAL SYSTEM

The lenses will be glued to a custom-made aluminium holder which allows their placement in front of the pump laser diode. Organic based epoxies not specified for operation under vacuum tend to outgas, which may result in material depositing on optical surfaces leading to transmission losses (Riede et al., 2011). As the system will need to operate in vacuum and high optical power is involved the glue selection resulted from a compromise between low outgassing and high thermal conductivity.. Stycast 2850ft with catalyst 9 was finally selected and its most relevant properties may be found in Table 3.

Table 3: Most Relevant Characteristics of the selected glue.

Thermal Conductivity (W/m.K)	TML* (%)	CVCM** (%)
1.25	0.25	0.001

*Total Mass Loss in vacuum
** Collected Volatile Condensable Materials

The lenses were placed on the holder with a customized clamp as depicted in Figure 6.

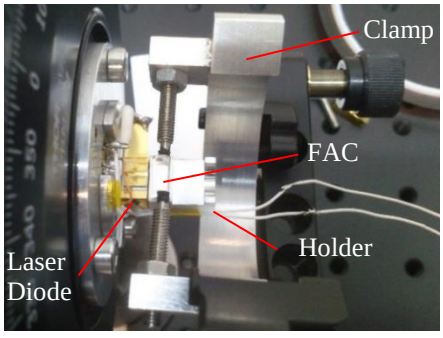

Figure 6: Detail of Lens Positioning Setup.

The clamp is connected to a kinematic mount and an xyz translation stage which allows the alignment to the propagation axis and its correct placement regarding the laser diode, respectively. The emission of the laser diode itself and a simplified wavefront sensor were used to evaluate the correct position of the collimator regarding it. Once a satisfactory position was reached the lenses were glued to the holder as depicted in Figure 7.

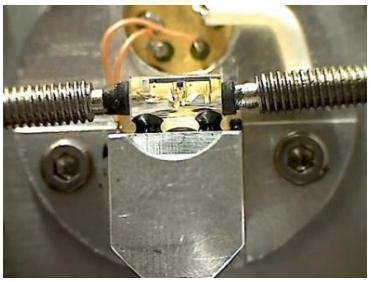

Figure 7: FAC during gluing process.

The method used for the experimental verification of the lens placement is further detailed in the next section of this paper.

3.1 Simplified Wavefront Sensor

A significant part of this optical system consists of collimating a divergent laser beam, wavefront sensing naturally arises as the means to assess the correct placement of the system's optics. However, developing a full wavefront reconstruction algorithm would exceed the time and cost frame of this project. So, a compromise solution was reached which consisted of assembling a 500µm pitch microlens array in front of a common cmos camera and using its live feed to monitor the laser beam divergence while adjusting the lens. The wide red beam of a K-Laser AK-100 surface inspection system was used to place the array at focal length from the cmos sensor and to align it parallel to the camera sensor. The reference position of the wavefront sensor could then be recorded. A red grid whose nodes are the said reference positions was superimposed to the video live feed as depicted in Figure 8.

The white dots on Figure 8 correspond to a sample laser beam being analysed by the developed wavefront sensor. The main assumption is that a perpendicularly incoming beam that is collimated will be focused onto the grid nodes corresponding to the microlenses it is incident upon.

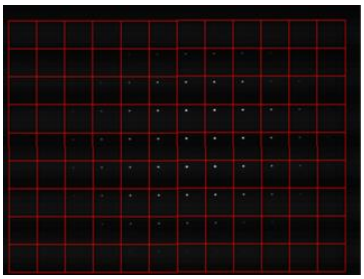

Figure 8: Sample beam reading by the developed wavefront sensor.

3.2 Lens Placement Results

The FAC was successfully placed at its collimating position with the aid of the wavefront sensor, from which the reading is presented in Figure 9 and with the aid of a DNT Digimicro 2.0 digital microscope which originated the picture in Figure 7.

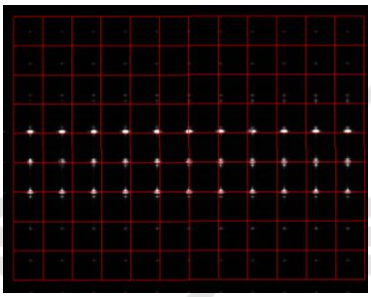

Figure 9: FAC Output as read by the wavefront sensor.

The picture in Figure 9 corresponds to the reading immediately after the glue was applied. Several other readings of the beam were taken throughout its 22-hour curing time and after clamps were removed showing very little alteration. A very slight increase of intensity of the focal spots on the lower row accompanied by the matching reduction on the lower one after some hours suggests that the lens descended during curing time which could be originated by glue contraction.

The beam ensuing from the FAC illuminating three consecutive rows of the wavefront sensor is consistent with the corresponding sequential and non-sequential simulations which indicate a vertical beam of 1.5mm at this stage. The SAC results were not as promising, they are depicted Figure 10.

Although a horizontal beam width of 1.5mm was also expected, it could not be achieved. Focal spots observed appear to be elongated on the horizontal direction and only because of that do they seem to overlap the reference grid, presenting a clear dispersion trend. Nevertheless, the SAC position that corresponds to the reading on Figure 10 was the one

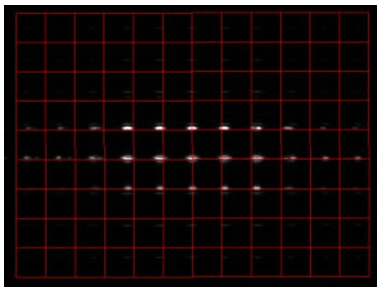

Figure 10: SAC Output as read by the wavefront sensor.

that minimized the amount of microlenses being illuminated in the horizontal direction. As such, the lens was glued in this position showing no visible alteration on the wavefront sensor reading during the respective curing time. A considerable amount of stray light appears to be present. Studies are underway to determine if this is so.

Finally, the FL was placed. As no camera was available at the time, its position was assessed by placing a fluorescent target flush with the end of the holder and then using the translation stage it was associated with to move the target to the system focal distance. The final system with all the lenses glued is presented in Figure 11.

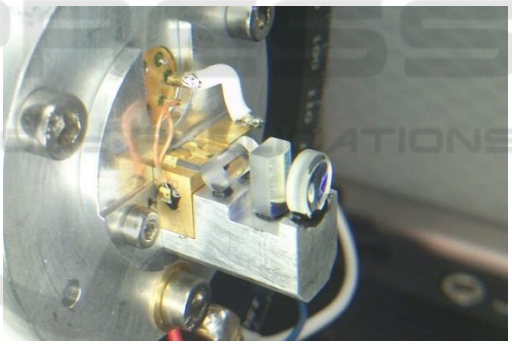

Figure 11: Fully assembled pumping system.

4 BEAM CHARACTERIZATION

The beam profile was characterized by placing a CCD camera associated with a XYZ translation stage facing the laser system and taking successive pictures at 0.1mm increments.

The fast and slow axis values of beam full width are plotted in Figure 12 alongside those of the non-sequential simulations.

It can be clearly seen that the point where the difference in width between fast and slow axis is minimized occurs at a shorter distance in the experimental values than for the simulated ones. In

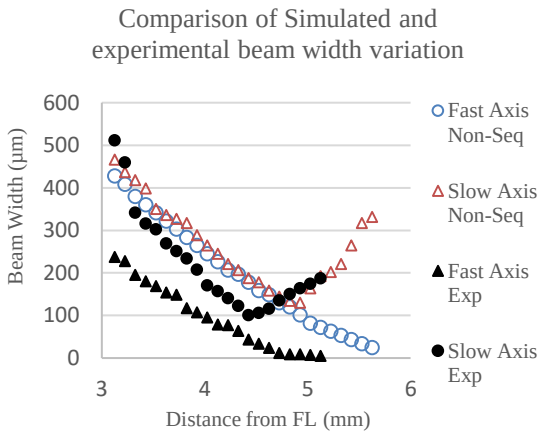

Figure 12: Comparison of beam width values experimental results with simulation values.

fact, at the 4.75mm design focal length, the beam is 11µmx135µm. At the point where the difference is minimized the beam is 43µmx97µm. This occurs at 4.43mm from the FL, which is within the active medium when placed at design position. The respective profile is presented in Figure 13.

Figure 13: Image of beam profile at 4.43mm from the FL.

This difference in focal length may arise from deficient method for assessing the FL position during gluing, as the naked eye observation of a fluorescent target may be misleading. The use of a CCD instead of the fluorescent target may prove a more assertive approach.

The horizontal lobes on the upper and lower limit of the focal area observed in the Non-Sequential simulation are also observable. However, a thin horizontal sliver in the middle section of the focal area is observed. This may be light that was not collimated by the SAC or perhaps diffused by its rough lateral surface.

5 CONCLUSIONS

A pump system based on an open emitter laser diode was designed using commercial easily available components. The component and adhesive selection allows simple adaptation to mission environment operation. The difference in divergence between the fast and slow axis, characteristic of this type of laser, was partially corrected by collimating each of the axis independently at the same width. Nevertheless, a focal spot, narrower than designed, was achieved still within the active medium. A thorough analysis of the beam profile near the optical spot was carried out and it could be concluded that further optimization is required since an improper placement impacts the energy concentration on the surface coatings of the active medium and may lead to coating damage. A simplified wavefront sensor was built and successfully used to assess the beam divergence during the placement of the collimators. The gluing process was successful with no discernible difference in wavefront reading at the end of the curing time.

ACKNOWLEDGEMENTS

The research presented in this paper is partially financed by Fundação para a Ciência e Tecnologia, through the PhD Scholarship PD/BD/114148/2016.

We would also like to acknowledge Dr. Manuel Abreu, Dr. João Pinto Coelho, Prof. José Figueiredo and Dr. David Alves for lending equipment and technical advice.

REFERENCES

Akhtar, S., Ashraf, M. and Khan, K., 2007. A study of neutron and gamma radiation effects on transmission A study of neutron and gamma radiation effects on transmission. *Optical Materials*, Volume 29, p. 1595–1603.

Bouguin, F. and Galstian, T., 2002. *In-Situ Recorded Holographic Lenses for Near Infrared Diode Lasers.* Santa Fe, Proc. SPIE 4342, Optical Data Storage 2001, (10 January 2002); .

ESRE, 2017. *Selected Trends and Space Technologies Expected to Shape the Next Decade*, Brussels: ESRE-Association of European Space Research Establishments.

Hamlin, S., Hays, A., Trussel, W. and King, V., 2004. *Eyesafe Erbium Glass Microlaser*. Bellingham, WA, s.n.

Hasan, N., Haque, M. and Lee, L., 2016. Deastigmatism, circularization, and focusing of a laser. *Optical Engineering*, 55(9), pp. 095107-1 to 095107-7.

Hitoshi, K. and Kawaguchi, J., 2011. *Lessons Learned from round Trip of HAYABUSA Asteroid Explorer in Deep Space.* Big Sky, IEEE Aerospace Conference(AERO).

Johansson, S. et al., 2007. Laser diode beam shaping with GRIN lenses using the twisted beam approach and its application in pumping of a solid-state laser. *Optics Communications*, 274(2), pp. 403-406.

Kemski, R., 2011. *Curiosity – The Mission and Parts Lessons.* European Space Components Conference (ESCCON), California Institute of Technology.

Manolis, I. et al., 2015. *Sensors, Systems, and Next-Generation Satellites XIX*. Toulouse, Proc. of SPIE Vol. 9639, 96391N.

Mlynczak, J. and Belghachem, N., 2015. Monolithic thermally bonded Er3+, Yb3+:glass/Co2+:MgAl2O4. *OpticsCommunications*, Volume 356, pp. 166-169.

Riede, W. et al., 2011. *Laser-induced contamination on space optics.* Boulder, Colorado, SPIE Laser Damage.

SoodBiswas, N., Sekh, A., Sarkar, S. and Basuray, A., 2012. Anamorphic gradient index (GRIN) lens for beam shaping. *Optics Communications*, Volume 285, p. 2607–2610.

Sun, H., 2015. *A Practical Guide to Handling Laser Diode Beams.* Pittsburgh: Springer.

Zayhowski, J. and Mooradian, A., 1989. Single-frequency microchip Nd lasers. *OPTICS LETTERS*, Vol. 14(No. 1), pp. 24-26.

Zayhowski, J., Ochoa, J. and Mooradian, A., 1989. Gain-switched pulsed operation of microchip lasers. *OPTICS LETTERS*, Vol. 14(No. 23), pp. 1318-1320.